PREDICTING FIRE HOTSPOTS IN KALIMANTAN BASED ON CLIMATE FACTORS USING GAUSSIAN PROCESS REGRESSION AND LONG SHORT-TERM MEMORY

Sri NURDIATI[1], Mochamad Tito JULIANTO[1], Ionel HAIDU[2,3], Muhammad Daryl FAUZAN[1], Hari NURDIANTO[1], Syukri Arif RAFHIDA[1] & Mohamad Khoirun NAJIB[1]*

DOI: 10.21163/GT_2026.212.02

ABSTRACT

Forest and land fires in Kalimantan present a recurrent environmental challenge, driven by local and global climatic factors. Predicting fire hotspots is crucial for mitigation efforts. This study compares the performance of Gaussian Process Regression (GPR) and Long Short-Term Memory (LSTM) networks in forecasting monthly fire hotspots based on six climatic indicators, including rainfall, dry spells, and ENSO and IOD indices. GPR models were developed using several kernels and hyperparameter tuning methods, while LSTM models applied multiple architectural configurations combined with regularisation techniques. The results show that while GPR models achieved good fitting on training data, they suffered from overfitting and lower accuracy during testing, even after optimisation. In contrast, the LSTM model with two LSTM layers and four dense layers demonstrated superior predictive performance, achieving a testing RMSE of 522.12 and an Explained Variance Score (EVS) of 0.834. LSTM effectively captured complex temporal patterns inherent in climate-driven fire hotspot data. Nevertheless, both models faced difficulties in predicting anomalies linked to socio-economic interventions, such as the significant reduction in fire hotspots in 2018.The findings highlight the effectiveness of LSTM in modelling temporally dependent environmental phenomena and suggest the need for integrating socio-economic variables into future predictive frameworks to improve robustness. This study contributes valuable insights towards enhancing early warning systems for forest fire risk management in Kalimantan and other tropical regions.

Keywords: *Fire hotspots; Kalimantan; Gaussian Process Regression; Long Short-Term Memory; Machine learning.*

1. INTRODUCTION

Kalimantan, the third largest island in the world with an area of 539,460 km² (MacKinnon & Hatta, 2013), frequently draws attention due to recurring environmental issues, notably forest and land fires (Sarmiasih & Pratama, 2019; Gusnita, 2021; Qirom et al., 2022; Saharjo & Hasanah, 2023). These events occur annually (Saharjo & Velicia, 2018), with major fire episodes recorded in 1982, 1997–1998, 2015, and 2019 (Najib et al., 2022; Werf et al., 2017). Forest fires have significant impacts, including ecosystem destruction, air pollution, public health risks, and economic losses estimated at approximately IDR 74 million per hectare (Ulya & Yunardy, 2006; Mulia et al., 2021; Sari et al., 2022; Wasis et al., 2019). Early indicators of forest fires can be identified through the presence of hotspots, defined as areas experiencing elevated surface temperatures associated with burning (Nugrahani et al., 2024; Reddy et al., 2019).

*[1] School of Data Science, Mathematics, and Informatics, IPB University, Bogor, Indonesia. * Corresponding author nurdiati@apps.ipb.ac.id (SN); mtjulianto@apps.ipb.ac.id (MTJ); ryls93daryl@apps.ipb.ac.id (MDF); ryls93daryl@apps.ipb.ac.id (HN); asrafhida@apps.ipb.ac.id (SAR); mkhoirun@apps.ipb.ac.id (MKN)*

[2] LOTERR (Laboratoire des Observations des Territoires), Université de Lorraine, F-57000 Metz, France. ionel.haidu@univ-lorraine.fr (IH).

[3] STAR-UBB (Scientific and Technological Advanced Research Institute), Babeș-Bolyai University, 400084 Cluj-Napoca, Romania.

Forest fires in Kalimantan are strongly influenced by both local and global climatic conditions. Variables such as air temperature, rainfall, and humidity are closely linked to hotspot occurrence (Saharjo & Velicia, 2018). Moreover, global climate phenomena such as the El Niño–Southern Oscillation (ENSO) and the Indian Ocean Dipole (IOD) play crucial roles in shaping weather and climate patterns across Indonesia (Ardiyani et al., 2023; Irwandi et al., 2019; Nurdiati et al., 2022; Rafhida et al., 2024). The ENSO phases, El Niño and La Niña, respectively prolong drought periods or enhance rainfall intensity, while the IOD influences rainfall distribution across regions (Anggraini & Trisakti, 2011; Bramawanto & Abida, 2017; Nurdiati et al., 2024).

Given the extensive impacts of forest fires, there is an urgent need to accurately predict the number of hotspots in Kalimantan. Reliable prediction models not only facilitate the identification of high-risk areas but also enable governments and other stakeholders to design effective mitigation strategies (Sudrajat & Subekti, 2019; Yuliarti & Anggraini, 2022). Although numerous predictive methods have been explored in previous studies, challenges remain in achieving accuracy and reliability, particularly when using climate indicators. Techniques such as autoregression (AR), artificial neural networks (ANN), support vector regression (SVR), random forest regression, and gradient boosting regression often struggle to effectively capture temporal patterns in the data (Nugrahani et al., 2024; Nurdiati, Sopaheluwakan, et al., 2022).

This study builds upon Najib et al. (2022) and (Nugrahani et al., 2024) by analysing a dataset consistent with their monthly BMKG hotspot counts on a 0.25° × 0.25° grid across Kalimantan for 2001–2020 with preprocessing that excludes persistently low-activity grids following Najib et al. (2021). Najib et al. (2022) utilised rainfall and dry spell indicators to predict hotspot abundance using copula regression, whereas Nugrahani et al. (2022) incorporated rainfall anomalies, as well as IOD and ENSO indices, applying various machine learning methods. However, previous research has yet to fully leverage these indicators within more sophisticated predictive models, particularly under Kalimantan's dynamic temporal conditions. It was also observed that the previous models exhibited significant overfitting, highlighting the need for more robust approaches.

In this study, two predictive methods are employed to model the number of hotspots based on climatic indicators: Gaussian Process Regression (GPR) and Long Short-Term Memory (LSTM) networks. GPR is renowned for its capability to model complex relationships between variables, particularly in small datasets. It has demonstrated superior predictive performance in various studies, often yielding lower fitting errors compared to alternative methods (Kamath et al., 2018). Furthermore, GPR has proven effective across applications such as remote sensing and weather data analysis (Hultquist et al., 2014; La Fata et al., 2024). According to Foley (2024) GPR is particularly advantageous for dealing with incomplete or noisy datasets, offering a probabilistic approach that explicitly quantifies prediction uncertainties—making it a promising option for modelling the relationship between climate indicators and forest fire hotspots.

Meanwhile, the LSTM deep learning algorithm has gained popularity in recent years for hotspot prediction tasks due to its proficiency in capturing complex temporal dependencies in time-series data (DiPietro & Hager, 2019; Kadir et al., 2022; Listia Rosa et al., 2022; Kadir et al., 2023; Luo et al., 2024; Li et al., 2024; Eaturu & Vadrevu, 2025). LSTM-based ensembles fused with (variance-weighted) Kalman filtering for environmental time series, supports the choice of LSTM for climate temporal signals and highlights the value of robust gap-filling before modelling (Haidu et al., 2025). LSTM represents an advancement over conventional Recurrent Neural Networks (RNNs), effectively addressing the "vanishing gradient" problem where gradients used to update network weights diminish or disappear (Noh, 2021). Research by Kadir et al. (2023) demonstrated that LSTM models could accurately predict the quantity and distribution of forest fire hotspots in Indonesia based on NASA MODIS datasets, achieving a mean percentage error of 6.94%. However, that study solely relied on past hotspot data without incorporating other climatic factors. The present study seeks to enhance prediction accuracy by integrating a range of climate indicators.

Through these two approaches, this research aims to evaluate the effectiveness of GPR and LSTM methods in predicting the number of hotspots in Kalimantan based on both local and global climate indicators. The study not only focuses on predictive accuracy but also explores the relative

strengths and weaknesses of each method. The main contribution of this research lies in providing empirical insights into which predictive method is more effective and reliable under the context of climate variability and the tropical environmental characteristics of Kalimantan. The findings are expected to inform the development of more robust predictive models for wildfire mitigation applications. Furthermore, this research contributes to practical policy formulation by offering data-driven recommendations to prevent and mitigate the impacts of forest fires in Kalimantan and other regions with similar environmental profiles.

2. STUDY AREA AND DATASETS

Kalimantan Island (5°S–7.25°N, 108°E–119.75°E), shared by three countries—Indonesia, Malaysia, and Brunei Darussalam—has attracted considerable attention in wildfire hotspot research. The Indonesian portion of the island comprises five provinces: West Kalimantan, Central Kalimantan, South Kalimantan, East Kalimantan, and North Kalimantan. Geographically, Kalimantan is characterised by extensive tropical rainforests, vast peatlands, and a humid tropical climate with consistently high temperatures and humidity throughout the year. The island accounts for approximately 33.8% of Indonesia's total peatland area, making it an ecologically significant yet highly fire-prone region.

Rainfall patterns across Kalimantan are classified into equatorial and monsoonal types. Areas experiencing a monsoonal pattern, particularly in the southern and central regions, are more susceptible to wildfires, especially during prolonged dry seasons intensified by El Niño events. Research indicates that strong El Niño events can extend the dry season, increase the number of consecutive dry days, and subsequently trigger a greater number of wildfire hotspots. Conversely, La Niña events, which bring more frequent rainfall, tend to reduce the risk of fires. The positive phase of the Indian Ocean Dipole (IOD), when occurring simultaneously with El Niño, can further exacerbate drought conditions.

Hotspot data used in this study were obtained from Indonesian Meteorological, Climatological, and Geophysical Agency (BMKG) as a distributor of satellite active-fire detections derived from MODIS (MOD14/MYD14) and VIIRS (e.g., VNP14IMG/VJ114IMG) products that implement the contextual active-fire detection algorithm. To ensure that the analysis focused on fire-prone areas, regions with consistently low hotspot activity, such as highland areas with high rainfall, were excluded. This approach follows the classification method proposed by Najib et al. (2021), in which Kalimantan's hotspot grids were clustered using the k-means (Lloyd, squared-Euclidean) on hotspot time series evaluating 8 clusters and designating the lowest-incidence cluster as the candidate for removal.

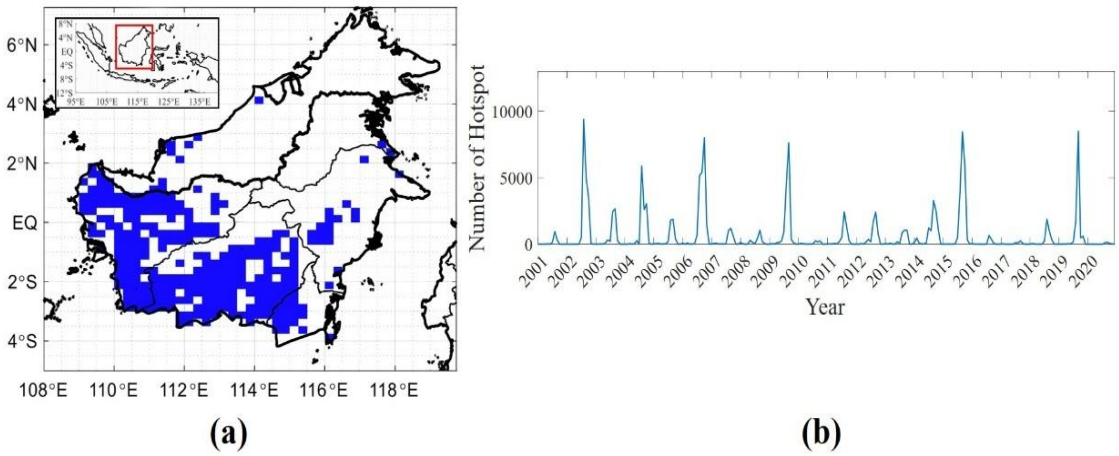

Fig. 1. (a) Kalimantan Island and selected research areas; (b) Total monthly hotspot counts.

Clusters characterised by extremely low fire incidence—with a maximum average of only 3.43 hotspots per grid point (e.g., in 2002)—were disregarded to avoid distorting the analysis of wildfire characteristics in Kalimantan.

Following Najib et al. (2021), we first excluded 0.25°×0.25° grid cells with persistently low hotspot activity using a k-means clustering of grid-level hotspot time series, and retained only high-incidence grids. This study only includes areas with significant hotspot concentrations, particularly in Central, South, and West Kalimantan, as shown in **figure 1(a)**. For each month between 2001 and 2020, hotspot counts were then summed over all retained grids, yielding a single monthly total hotspot count. Analysis was conducted using total monthly hotspot data from 2001 to 2020, illustrated in **figure 1(b)**. The trend in hotspot numbers exhibits a clear seasonal cycle, with peaks typically occurring mid-year and lower counts during the rest of the year. The number of hotspots tends to increase during the dry season, especially between July and September, due to low humidity and minimal rainfall. In contrast, during the rainy season, the number of hotspots declines significantly.

This study employed both local and global climatic factors to predict monthly total hotspot counts. Local climatic variables analysed included total rainfall, rainfall anomalies, and the number of dry days (defined as days with less than one millimetre of rainfall), extracted from the CMORPH dataset available from the National Oceanic and Atmospheric Administration (NOAA). Meanwhile, global climatic factors considered were indices related to the ENSO and IOD phenomena, obtained from NOAA. As a result, our dataset consists of a univariate target time series of regional hotspot totals and a corresponding multivariate time series of six aggregated climatic predictors; both the GPR and LSTM models are trained on this aggregated series rather than on individual grid-cell time series. Consequently, six independent variables were used in this research, with 80% of the data allocated for model training and the remaining 20% for testing.

Prior to model fitting, each of the six climatic predictor variables was standardised to zero mean and unit variance. The standardisation parameters (mean and standard deviation) were estimated exclusively from the training period (2001–2016) and then applied unchanged to the held-out test period (2017–2020). For the 16-fold cross-validation used in the GPR experiments, standardisation was recomputed in each fold by fitting the scaler on the 15 training years and applying it to the left-out validation year. For the LSTM models, lagged inputs from t–1 to t–12 was generated from these standardised predictor series, ensuring that all input windows were derived from features scaled using training-only statistics. The target variable, monthly hotspot counts, was retained in its original units without normalisation.

3. METHODS

This study employs two machine learning methods to predict the number of hotspots in Kalimantan, namely Gaussian Process Regression and Long Short-Term Memory.

3.1. Gaussian Process Regression

Gaussian Process (GP) is a widely used statistical method for data fitting and prediction based on machine learning. A GP is a form of stochastic process, defined as a collection of random variables Y indexed by an input space X, where any finite subset of these variables follows a multivariate Gaussian distribution (Rasmussen & Williams 2019). Gaussian Process Regression (GPR) is a non-parametric, Bayesian approach to regression, offering high flexibility in handling non-linear relationships between input and output variables.

A GPR model is fully characterised by a mean function $m(\mathbf{x})$ and a covariance function (kernel) $k(\mathbf{x}_i, \mathbf{x}_j)$,, defined as follows:

$$m(\mathbf{x}) = \mathbb{E}[\boldsymbol{Y}_{\boldsymbol{x}}], \tag{1}$$

$$k(\boldsymbol{x}_i, \boldsymbol{x}_j) = \mathbb{E}\left[\left(\boldsymbol{Y}_{\boldsymbol{x}_i} - m(\boldsymbol{x}_i)\right)\left(\boldsymbol{Y}_{\boldsymbol{x}_j} - m(\boldsymbol{x}_j)\right)\right]. \quad (2)$$

The only requirement for a valid kernel is that it must produce a positive semi-definite covariance matrix for any set of input points. Through this matrix, a Gaussian process can make predictions at new points based on information from the training data.

In the Bayesian regression framework, GPR models the relationship between input $\mathbf{x}_i$ and output y_i as:

$$y_i = f(\mathbf{x}_i) + \epsilon_i, \quad (3)$$

where ϵ_i represents Gaussian noise with zero mean and variance σ^2. The function f over the input space is given a multivariate Gaussian prior distribution with zero mean and covariance matrix $\mathbf{K}$:

$$f|\mathbf{X}, \theta \sim N(\mathbf{0}, \mathbf{K}). \quad (4)$$

For prediction, GPR provides a Gaussian distribution for each array of new input variables $\mathbf{X}^* = [\mathbf{x}_1^*, \mathbf{x}_2^*, \ldots, \mathbf{x}_n^*]$. The estimated value for y^* is $m(\mathbf{X}^*)$ and the variance of y^* is given by $\mathrm{cov}(\mathbf{X}^*)$. In kernel space, the mean and covariance prediction equations are:

$$m(\mathbf{X}^*) = \mathbf{k}^{*\mathrm{T}}(\mathbf{K} + \sigma^2\boldsymbol{I})^{-\mathbf{1}}\mathbf{y}, \quad (5)$$

$$\mathrm{cov}(\mathbf{X}^*) = k(\mathbf{X}^*, \mathbf{X}^*) - \mathbf{k}^{*\mathrm{T}}(\mathbf{K} + \sigma^2\mathbf{I})^{-\mathbf{1}}\mathbf{k}^*, \quad (6)$$

where $\mathbf{k}^*$ is the covariance vector between the new data $\mathbf{X}^*$ and the training data.

3.1.1. Hyperparameter Tuning

In machine learning, parameters that are not updated during model training and must be configured beforehand are known as hyperparameters. Model performance can vary significantly depending on the choice of hyperparameters; hence, careful tuning is crucial. In GPR, the noise level σ^2 is treated as a hyperparameter that can be optimised. Noise level refers to the variation or uncertainty in observations, represented as the variance of the added Gaussian noise (Li et al., 2020). In this study, tuning of the noise level was conducted using several optimisation methods, following (Rasmussen & Williams, 2019), namely maximum marginal likelihood (MML), Bayesian optimisation, grid search, and random search.

1. Maximum Marginal Likelihood

The marginal likelihood function is obtained by integrating the likelihood function multiplied by the prior distribution of f:

$$p(\boldsymbol{y}|\mathbf{X}, \boldsymbol{\theta}) = \int p(\boldsymbol{y}|\mathbf{f}, \mathbf{X}, \boldsymbol{\theta}) p(\mathbf{f}|\mathbf{X}, \boldsymbol{\theta})\, d\mathbf{f}, \quad (7)$$

where $\boldsymbol{y}$ represents the observed response variable, $\mathbf{X}$ is the matrix of observed inputs, $\boldsymbol{\theta}$ denotes the model parameters, and $\mathbf{f}$ is the function representing the relationship between $\mathbf{X}$ and $\boldsymbol{y}$. Within the Gaussian Process framework, the prior distribution $\mathbf{f}|\mathbf{X}, \boldsymbol{\theta}$ is multivariate Gaussian, $\mathbf{f}|\mathbf{X}, \boldsymbol{\theta} \sim N(\mathbf{0}, \mathbf{K})$.

2. Bayesian optimization

Bayesian optimisation relies on a surrogate function to locate the best parameter values (Ye et al., 2019). The surrogate function uses a probabilistic model that is updated with new information. It works by identifying regions likely to contain the optimum and sampling points close to these regions to refine the model. In this context, Gaussian processes are used as surrogate functions for the objective function.

The probability of the objective function is evaluated using an acquisition function (Ye et al., 2019), commonly the expected improvement (EI), defined as:

$$EI_{y^*}(x) = \int_{-\infty}^{\infty} max(y^* - y, 0)\, p(y|x, \boldsymbol{\theta}) dy, \quad (8)$$

where x is the input, y^* is the best observed value, y is the model's predicted value, and $p(y|x, \boldsymbol{\theta})$ is the posterior distribution.

3. Grid Search

Grid search is a hyperparameter search technique that systematically tries all combinations within a specified parameter space. It constructs a grid of parameter values and evaluates the model performance at each grid point.

4. Random Search

Random search selects hyperparameter combinations randomly within a defined search space. Unlike grid search, it does not exhaustively explore all combinations but samples a predefined number of configurations.

3.1.2. Kernel Selection

As introduced earlier, GPR relies on kernels to make predictions at new points. The kernel functions as a covariance function measuring the similarity between two points in input space. The choice of an appropriate kernel is crucial as it determines how the model captures patterns in the data, especially when the relationship is non-linear. This study employed three kernels: the exponential kernel, the squared exponential (Gaussian) kernel, and the Matern 3/2 kernel. In addition, we used variations of these kernels with Automatic Relevance Determination (ARD), which introduces separate length-scales for each explanatory variable. ARD enhances the model's adaptability by allowing each input dimension to have its own scaling parameter (Rasmussen & Williams, 2019). The original kernels and their ARD versions are summarised as in **table 1.**

Table 1.

Kernel Used in Study.

Kernel	Original	ARD
Exponential	$\sigma_f^2 \exp\left(-\frac{\lvert \mathbf{x}_i - \mathbf{x}_j \rvert}{\sigma_l}\right)$	$\sigma_f{}^2 \exp\left(-\sqrt{\sum_{m=1}^{d} \frac{(\mathbf{x}_{im} - \mathbf{x}_{jm})^2}{\sigma_{lm}{}^2}}\right)$
Squared Exponential (Gaussian)	$\sigma_f{}^2 \exp\left(-\frac{1}{2}\frac{\lvert \mathbf{x}_i - \mathbf{x}_j \rvert^2}{\sigma_l{}^2}\right)$	$\sigma_f{}^2 \exp\left(-\frac{1}{2}\sqrt{\sum_{m=1}^{d} \frac{(\mathbf{x}_{im} - \mathbf{x}_{jm})^2}{\sigma_{lm}{}^2}}\right)$
Matern3/2	$\sigma_f{}^2 \left(1 + \frac{\sqrt{3}}{\sigma_l} r\right) \exp\left(-\frac{\sqrt{3}}{\sigma_l} r\right)$	$\sigma_f{}^2 \left(1 + \frac{\sqrt{3}}{\sigma_l} r_{ard}\right) \exp\left(-\frac{\sqrt{3}}{\sigma_l} r_{ard}\right)$

where:

- $\mathbf{x}_i$ represents the training data,
- $\mathbf{x}_j$ denotes the testing data,
- σ_f is the signal standard deviation,
- σ_{lm} is the length-scale parameter for the mmm-th explanatory variable,
- d is the number of explanatory variables, and
- r and r_{ard} represent the Euclidean distance between $\mathbf{x}_i$ and $\mathbf{x}_j$ for standard and ARD kernels, respectively.

3.2. Long Short-Term Memory (LSTM)

The Long Short-Term Memory (LSTM) model is a type of Recurrent Neural Network (RNN) designed for time series data that exhibits dependencies on previous observations. The output from prior steps is used to update new weight values. These updated weights are then applied in subsequent computations, establishing a connection between new and prior data.

The LSTM model was specifically designed to overcome the limitations of conventional RNNs, which often struggle with long-range dependencies and are prone to the vanishing and exploding gradient problems [36]. LSTM represents a specialised architecture within the RNN family. Unlike a simple RNN, the hidden units of an LSTM consist of three principal gates: the forget gate, the input gate, and the output gate. The mathematical formulations of the *forget gate* $f^{(t)}$(8), *input gate* $i^{(t)}$ (9), *output gate* $o^{(t)}$ (10), candidate *cell state* $\tilde{C}$(11), *cell state* C (12), and *hidden layer* $h^{(t)}$ (13) are as follow:

$$\boldsymbol{f^{(t)}} = \sigma(\boldsymbol{W_f x_t} + \boldsymbol{W_f h^{(t-1)}} + \boldsymbol{\theta_f}) \tag{9}$$

$$\boldsymbol{i^{(t)}} = \sigma(\boldsymbol{W_i x_t} + \boldsymbol{W_i h^{(t-1)}} + \boldsymbol{\theta_i}) \tag{10}$$

$$\boldsymbol{o^{(t)}} = \sigma(\boldsymbol{W_o x_t} + \boldsymbol{W_o h^{(t-1)}} + \boldsymbol{\theta_o}). \tag{11}$$

$$\boldsymbol{\widetilde{C}^{(t)}} = tanh\big(\boldsymbol{W_c x_t} + \boldsymbol{W_c h^{(t-1)}} + \boldsymbol{\theta_c}\big) \tag{12}$$

$$\boldsymbol{C^{(t)}} = \boldsymbol{f^{(t)}} \cdot \boldsymbol{C^{(t-1)}} + \boldsymbol{i^{(t)}} \cdot \boldsymbol{\widetilde{C}^{(t)}} \tag{13}$$

$$\boldsymbol{h^{(t)}} = \boldsymbol{o^{(t)}} \cdot tanh\,(\boldsymbol{W_c C^{(t)}} + \boldsymbol{\theta_h}) \tag{14}$$

where $\boldsymbol{W_f, W_i, W_o}$, and $\boldsymbol{W_h}$ represent the weight matrices for the forget gate, input gate, output gate, and hidden layer, respectively. Likewise, $\boldsymbol{\theta_f, \theta_i, \theta_o}$ and $\boldsymbol{\theta_h}$ are the biases associated with each corresponding gate.

The weights and biases in the model must be initialised prior to the training process. Glorot, Bengio (2010) introduced the *Glorot uniform* initialisation method, which sets the initial weights based on a uniform distribution. This method is widely adopted for initialising weights in deep learning models. By default, the TensorFlow package in the Python programming language applies the Glorot uniform method for weight initialisation. The distribution of weights using the Glorot uniform method is defined by:

$$W \sim U\left(-\frac{\sqrt{6}}{\sqrt{n_{in}+n_{out}}}, \frac{\sqrt{6}}{\sqrt{n_{in}+n_{out}}}\right) \tag{15}$$

where n_{in} is the number of input units, and n_{out} is the number of output units. In addition, the biases are initialised to zero.

Each gate utilises either the sigmoid function σ or the hyperbolic tangent (tanh) function. The sigmoid activation outputs values within the interval $[0,1]$, controlling whether information is retained or discarded: an output close to 0 implies forgetting, whereas an output close to 1 implies retaining the information. An illustration of the LSTM architecture is presented in **figure 2**.

In this study, the LSTM model architecture is enhanced with regularisation techniques to improve performance and prevent overfitting by early stopping after 25 epochs. Early stopping monitors model performance during training and halts the process once the loss function ceases to improve after a pre-specified patience value (s epochs). This method helps prevent the model from overtraining and becoming trapped in local minima, thereby mitigating overfitting.

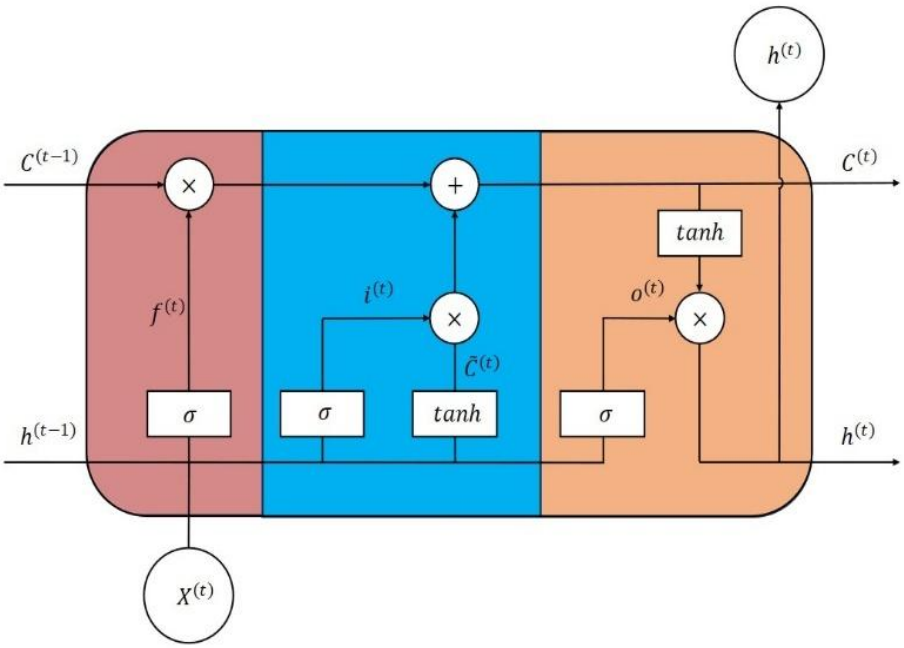

Fig. 2. LSTM model architecture.

3.3. Model Performance Metrics

To evaluate the performance of the machine learning (ML) model in predicting hotspots on the test data, two primary metrics are employed: the Root Mean Squared Error (RMSE) and the Explained Variance Score (EVS).

The RMSE measures the average squared difference between the observed and predicted values and is defined as:

$$\text{RMSE} = \sqrt{\frac{1}{n}\sum_{i=1}^{n}(\boldsymbol{y}^{(i)} - \hat{\boldsymbol{y}}^{(i)})^2}, \tag{14}$$

where $\boldsymbol{y}$ denotes the true values and $\hat{\boldsymbol{y}}$ represents the predicted values. The RMSE ranges from $[0, \infty)$ a value of 0 indicating a perfect prediction. A smaller RMSE value implies better predictive performance and higher accuracy.

Meanwhile, the EVS measures the proportion of variance in the actual values that is captured by the model's predictions. According to Oyedele et al. (2023), the explained variance score is defined as:

$$\text{EVS} = 1 - \frac{Var(\boldsymbol{y}-\hat{\boldsymbol{y}})}{Var(\boldsymbol{y})}. \tag{15}$$

where $Var(\cdot)$ denotes variance. The EVS ranges from $(-\infty, 1]$, with values closer to 1 indicating that the model explains nearly all of the variability in the data, reflecting excellent predictive performance.

4. RESULT

This section presents the evaluation results for both training and testing datasets.

4.1. Gaussian Process Regression

4.1.1. Kernel Selection

Gaussian Process Regression (GPR) was employed to predict fire hotspot occurrences from 2001 to 2020, based on six climate factors. Numerous kernel functions are available for GPR modelling, as they can be combined with other kernels. Consequently, identifying the most appropriate kernel function for the model is not straightforward. In this study, several commonly used kernels were examined: the Squared Exponential, ARD Squared Exponential, Matern32, and ARD Matern32 kernels.

In the initial stage, the most basic optimisation approach, namely maximal marginal likelihood (MML), was used to optimise the hyperparameters for each kernel. The results are presented in **table 2.**

Table 2.

Gaussian Process Regression Optimization Metric Evaluation.

Case	RMSE	
	Train	**Test**
GPR with Squared Exponential kernel	492.06	1116.9
GPR with ARD Squared Exponential kernel	501.29	971.27
GPR with Matern32 kernel	402.48	1133.5
GPR with ARD Matern32kernel	144.1	1227.3

Based on **table 2**, the ARD Matern32 kernel exhibited excellent performance on the training dataset, achieving a very low RMSE value. However, this high level of accuracy may indicate overfitting. This is further confirmed by the significant performance deterioration observed on the testing dataset, where the ARD Matern32 kernel produced the worst result compared to other kernels.

Thus, selecting an appropriate kernel function is crucial, as a good kernel should not only achieve high accuracy on the training data but also maintain good performance when predicting new data. Based on the consistency of the RMSE values between training and testing, the ARD Squared Exponential kernel was identified as the most relevant and robust choice for modelling the number of fire hotspots. Its consistent performance helps mitigate overfitting, making it a suitable option for this study.

4.1.2. Model Optimisation with Cross-Validation and Hyperparameter Tuning

While setting initial values and applying MML can optimise the marginal likelihood and enhance model accuracy, this approach alone is insufficient to fully address overfitting. To further improve the model, hyperparameter tuning was performed.

Prior to optimisation, a 16-fold cross validation from 16 years train data (2001-2016) technique was applied, partitioning the data by year to create 16 annual data groups. In this process, for the first fold, the data from 2001 were used for testing and the remaining years for training; for the second fold, 2002 data were used for testing, and so on, until each year's data had served as the test set once.

Hyperparameter tuning was then conducted using three optimisation methods: Bayesian optimisation, grid search, and random search. The evaluation results from these methods were compared to identify the best-performing model. The hyperparameter targeted for tuning was the noise variance (error variance), focusing on a low-complexity optimisation approach by adjusting only this single hyperparameter. The results are presented in **table 3**.

Table 3.

Gaussian Process Regression Optimisation Metric Evaluation.

Optimization	RMSE		EVS	
	Train	Test	Train	Test
Bayesian Optimization	700.93	**844.47**	0.805	**0.608**
Grid Search	713.78	853.09	0.798	0.593
Random Search	**694.97**	846.58	**0.808**	0.606

As shown in **table 3**, Bayesian optimisation achieved the best overall performance. It produced a training RMSE of 700.93 and a testing RMSE of 844.47, with corresponding EVS values of 0.805 and 0.608. These results suggest that Bayesian optimisation provides the best balance between training generalisation and the ability to explain data variability, making it a reliable method for predicting fire hotspot numbers.

Random search also demonstrated competitive performance, with the lowest training RMSE (694.97) and similar testing performance (RMSE 846.58, EVS 0.606). Grid search, on the other hand, showed slightly inferior performance compared to the other two methods. Based on these findings, Bayesian optimisation was selected as the most appropriate method for optimising the GPR model in this study, with random search as a viable alternative.

4.2. Long Short-Term Memory

Similar to the GPR approach, Long Short-Term Memory (LSTM) was employed to predict fire hotspots from 2001 to 2020 using the climate factors described in the dataset section. Using a window size of 12 months, the independent variables included all predictor variables from lag t–1 to t–12, while the dependent variable was the number of hotspots at time t. The LSTM model was built using the parameters outlined in t**able 4**.

Table 4.

LSTM Model Parameter.

PARAMETER	SPECIFICATION	DESCRIPTION
Loss function	RMSE	Experimental
Optimizer	Nadam	(Nurdiati, Najib, et al., 2022)
Learning rate	0.001	Experimental
Weight initializer	Glorot Uniform	(Glorot & Bengio, 2010)
Max epoch	500	(Abbasimehr & Paki, 2022)
Patience	25	(Terry et al., 2021)

The model architecture comprised combinations of LSTM layers and dense layers. Variations included one or two LSTM layers (with many-to-one or many-to-many schemes) and between one and four dense layers. The LSTM layers used the tanh and sigmoid activation functions, while the dense layers used ReLU activations.

Training was conducted using backpropagation, with early stopping applied if no improvement in testing loss was observed after 25 epochs. To address potential issues arising from poor weight initialisation by the Glorot Uniform method, the model was trained 20 times. The evaluation results for the LSTM method are shown in **table 5**.

Table 5.

LSTM Model Architecture Evaluation.

Architecture	RMSE		EVS	
	Train	Test	Train	Test
1 LSTM 1 Dense	725.02	899.17	0.808	0.521
1 LSTM 2 Dense	506.05	911.31	0.905	0.495
1 LSTM 3 Dense	382.48	646.61	0.945	0.746
1 LSTM 4 Dense	389.97	799.79	0.943	0.620
2 LSTM 1 Dense	825.82	862.77	0.755	0.544
2 LSTM 2 Dense	399.06	828.62	0.938	0.580
2 LSTM 3 Dense	678.61	811.47	0.826	0.613
2 LSTM 4 Dense	**343.01**	**522.12**	**0.956**	**0.834**

The evaluation results in **table 5** show that the "2 LSTM 4 Dense" architecture achieved the best performance among all variations tested. It recorded the lowest RMSE on the testing dataset (522.12) and the highest EVS (0.834), indicating excellent accuracy in predicting the number of fire hotspots and explaining a substantial portion of data variability.

Moreover, it demonstrated strong performance on the training dataset (RMSE 343.01, EVS 0.956), suggesting its capability to capture historical data patterns effectively. Conversely, simpler architectures such as "1 LSTM 1 Dense" exhibited significantly lower performance, with a high testing RMSE (899.17) and a low EVS (0.521), indicating insufficient ability to capture the complexity of the temporal data. Although architectures with more dense layers generally showed performance improvements, these results highlight the importance of using additional LSTM layers to better capture complex temporal relationships. Thus, the "2 LSTM 4 Dense" architecture was identified as the optimal choice for predicting fire hotspot numbers based on climatic factors in this study.

4.3. Best Model

The best-performing models identified in the previous sections—GPR with Bayesian optimisation and LSTM with a two-layer LSTM and four dense layers architecture—were compared against the actual data, as shown in f**igure 3**.

Figure 3 visualises the comparison between the prediction results of the two models, where (a) GPR predictions are shown in red and (b) LSTM predictions in blue, against the actual data. It should be noted that the LSTM model utilises lagged inputs; thus, predicting at time *t* requires data from *t-12* to *t-1*, which results in no predictions being made for the year 2001.

It is evident that the LSTM model outperforms GPR in predicting the number of fire hotspots, both on training and testing datasets, particularly during spike periods in the dry season. The GPR model tends to underestimate the peak number of hotspots during major spike years in the training data, notably in 2002, 2004, 2006, 2009, and 2015. In contrast, the LSTM model successfully captures these peak events within the training period.

However, both models demonstrate limitations in predicting peak hotspot numbers within the testing data. GPR notably overestimated the number of hotspots in 2018, while LSTM overestimated in 2017 and underestimated in 2019, although it performed reasonably well in predicting the hotspot count for 2018. Previous research (Gunadi et al., 2019) indicated that the decline in hotspot numbers in 2018 was due to efforts aimed at supporting the Asian Games held in Indonesia.

Furthermore, study (Nugrahani et al., 2024) reported that four different models tended to overestimate hotspot occurrences during that year, consistent with the overestimation observed in the GPR model. This discrepancy arises because machine learning models primarily rely on historical patterns for predictions and typically do not account for real-world socioeconomic factors. Nevertheless, the LSTM model, by incorporating temporal lags, appears to capture patterns more closely related to recent data preceding the prediction period.

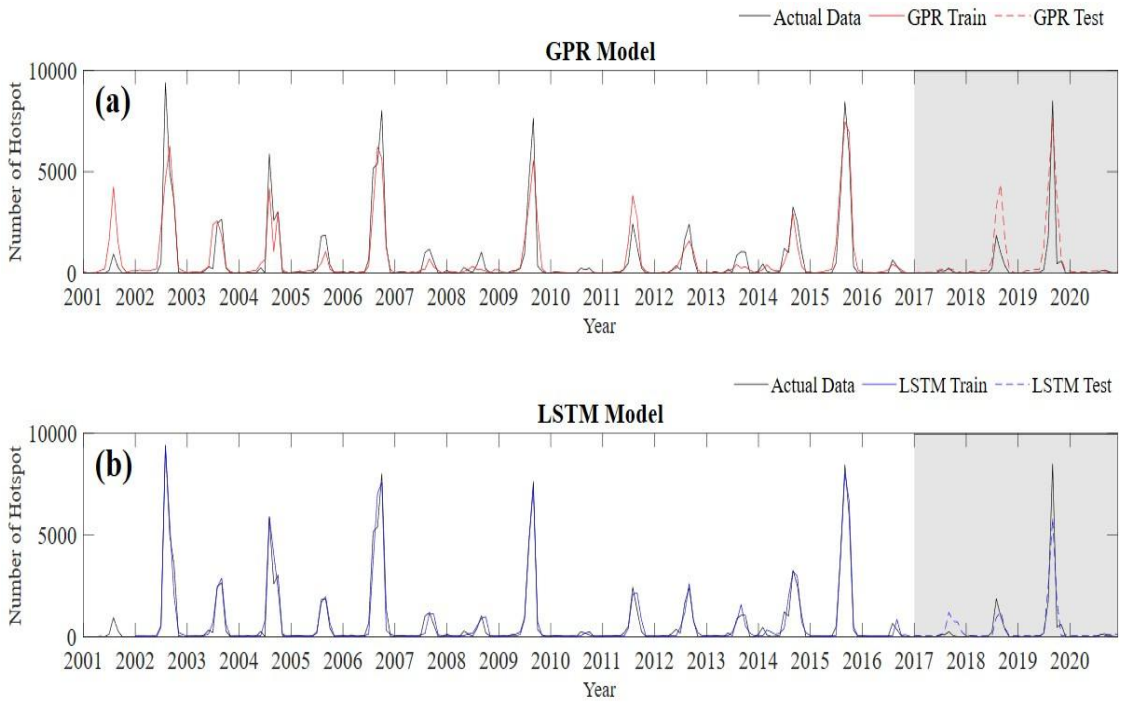

Fig. 3. Prediction comparison between GPR and LSTM.

5. DISCUSSION

The comparative analysis between Gaussian Process Regression (GPR) and Long Short-Term Memory (LSTM) models in this study reveals insightful findings on the challenges and strengths of each method when applied to the prediction of forest fire hotspots in Kalimantan using climate factors. Notably, the LSTM architecture with two LSTM layers and four dense layers produced the most accurate results, achieving a testing RMSE of 522.12 and an EVS of 0.834. This performance highlights LSTM's superior ability to capture complex temporal dependencies, especially in climate-driven phenomena that are seasonal and nonlinear.

This finding supports Kadir et al. (2023), who also found LSTM effective for hotspot forecasting in Indonesia, achieving an average error of only 6.94% even when using simpler models based solely on past hotspot counts. The present study builds upon that by integrating six climate predictors—including rainfall, dry spells, ENSO, and IOD—thus expanding the model's explanatory power. The enhanced accuracy confirms that including relevant climate variables strengthens LSTM's generalization, especially when paired with effective regularization techniques such as dropout and early stopping.

In contrast, GPR demonstrated solid performance during training but experienced a notable decline in accuracy on test data, particularly when complex kernels like ARD Matern32 were used. This suggests an overfitting issue, a phenomenon also discussed by Kamath et al. (2018), who found GPR highly accurate but sensitive to hyperparameter settings and prone to overfitting in high-complexity domains. Although GPR showed some generalization improvement with Bayesian optimization, its testing RMSE (844.47) and EVS (0.608) remained well below that of the best-performing LSTM model.

Similar concerns were raised in Hultquist et al. (2014), where GPR was outperformed by Random Forests in predicting burn severity due to its relative inflexibility with noisy and high-dimensional remote sensing data. These findings collectively suggest that while GPR has strong theoretical appeal—especially with its uncertainty quantification and Bayesian foundation—it may fall short in real-world applications involving dynamic temporal and multivariate data like wildfire hotspot prediction.

Luo et al. (2024) further validate the LSTM architecture's strength, demonstrating its capacity to forecast methane emissions with high fidelity in multivariate time series scenarios. Their findings align with this study's conclusion that LSTM can effectively model complex environmental systems where variables are interdependent and evolve over time. The success of deeper architectures (e.g., 2 LSTM + 4 dense layers) indicates that the model's depth and capacity play a crucial role in capturing spatiotemporal nuances in climate data.

However, one consistent limitation across studies—including this one—is the inability to predict sociopolitical anomalies, such as the significant decrease in hotspots in 2018 due to government efforts to reduce fires during the Asian Games. Gunadi et al. (2019) highlight the critical role of policy in shaping fire outcomes, suggesting that models based purely on environmental predictors will struggle to account for such interventions. This was evident when GPR overestimated and LSTM underestimated fire counts for certain years—both reflecting the models' reliance on historical climatic patterns without sociopolitical context. The example of South Africa (Madondo et al., 2023), regionally different, but it supports the claim that socio-economic and governance interventions can create anomalies versus climate-only predictors.

In conclusion, the study underscores the potential of LSTM for operational forest fire forecasting, especially when enriched with relevant climatic inputs. Meanwhile, GPR remains valuable for theoretical modeling and applications requiring probabilistic interpretation. Future research should explore hybrid modeling approaches that combine the temporal learning strengths of LSTM with the uncertainty quantification of GPR, while also integrating socioeconomic variables to capture the full spectrum of fire dynamics in Kalimantan and similar fire-prone regions.

6. CONCLUSION

This study successfully demonstrated that both Gaussian Process Regression (GPR) and Long Short-Term Memory (LSTM) models can be employed to predict the number of fire hotspots in Kalimantan based on climate factors. Through model development and evaluation, the LSTM model with two LSTM layers and four dense layers achieved superior performance, with a testing RMSE of 522.12 and an EVS of 0.834, indicating a strong capability to capture temporal patterns in climate and fire data. The GPR model, although effective with Bayesian optimization, was less capable of handling the complex temporal dependencies compared to LSTM. The research underscores the importance of selecting models that can adapt to the temporal dynamics inherent in climate-induced fire risks. Future studies may explore integrating socio-economic variables and higher-resolution climate forecasts to further enhance the predictive performance and operational applicability of fire hotspot prediction models in Kalimantan and similar tropical regions.

REFERENCES

Abbasimehr, H., & Paki, R. (2022). Improving time series forecasting using LSTM and attention models. *Journal of Ambient Intelligence and Humanized Computing*, *13*(1), 673–691. https://doi.org/10.1007/s12652-020-02761-x

Anggraini, N., & Trisakti, B. (2011). Kajian dampak perubahan iklim terhadap kebakaran hutan dan deforestasi di provinsi Kalimantan Barat. *Jurnal Penginderaan Jauh Dan Pengolahan Data Citra Digital*, *8*.

Ardiyani, E., Nurdiati, S., Sopaheluwakan, A., Septiawan, P., & Najib, M. K. (2023). Probabilistic Hotspot Prediction Model Based on Bayesian Inference Using Precipitation, Relative Dry Spells, ENSO and IOD. *Atmosphere*. https://doi.org/10.3390/atmos14020286

Bramawanto, R., & Abida, R. F. (2017). Tinjauan Aspek Klimatologi (ENSO dan IOD) dan Dampaknya Terhadap Produksi Garam Indonesia. *Jurnal Kelautan Nasional*. https://doi.org/10.15578/jkn.v12i2.6061

DiPietro, R., & Hager, G. D. (2019). Deep learning: RNNs and LSTM. In *Handbook of Medical Image Computing and Computer Assisted Intervention*. https://doi.org/10.1016/B978-0-12-816176-0.00026-0

Eaturu, A., Vadrevu, K.P. (2025). Evaluation of machine learning and deep learning algorithms for fire prediction in Southeast Asia. *Sci Rep* **15**, 18807. https://doi.org/10.1038/s41598-025-00628-9

Foley, E. (2024). Leveraging Gaussian Processes in Remote Sensing. *Energies*, *17*(16). https://doi.org/10.3390/en17163895

Glorot, X., & Bengio, Y. (2010). Understanding the difficulty of training deep feedforward neural networks. *Journal of Machine Learning Research*.

Gunadi, A., Gunardi, G., & Martono, M. (2019). THE LAW OF FOREST IN INDONESIA: PREVENTION AND SUPPRESSION OF FOREST FIRES. *Bina Hukum Lingkungan*. https://doi.org/10.24970/bhl.v4i1.86

Gusnita, D. (2021). Impact of Forest Fires in Sumatra and Kalimantan to Atmospheric Pollution During Period Of 2010-2015. *JKPK (Jurnal Kimia Dan Pendidikan Kimia)*. https://doi.org/10.20961/jkpk.v6i1.35027

Haidu, I., Magyari-Sáska, Z., & Magyari-Sáska, A. (2025). Spatio-Temporal Gap Filling of Sentinel-2 NDI45 Data Using a Variance-Weighted Kalman Filter and LSTM Ensemble. *Sensors*, *25*(17). https://doi.org/10.3390/s25175299

Hultquist, C., Chen, G., & Zhao, K. (2014). A comparison of Gaussian process regression, random forests and support vector regression for burn severity assessment in diseased forests. *Remote Sensing Letters*. https://doi.org/10.1080/2150704X.2014.963733

Irwandi, H., Syamsu Rosid, M., & Mart, T. (2019). Identification of the El Niño Effect on Lake Toba's Water Level Variation. *IOP Conference Series: Earth and Environmental Science*, *406*(1). https://doi.org/10.1088/1755-1315/406/1/012022

E. A. Kadir, H. T. Kung, S. L. Rosa, A. Sabot, M. Othman and M. Ting, "Forecasting of Fires Hotspot in Tropical Region Using LSTM Algorithm Based on Satellite Data," *2022 IEEE Region 10 Symposium (TENSYMP)*, Mumbai, India, 2022, pp. 1-7, doi: 10.1109/TENSYMP54529.2022.9864407.

Kadir, E. A., Kung, H. T., Rosa, S. L., Sabot, A., Othman, M. & Ting, M. (2022). Forecasting of Fires Hotspot in Tropical Region Using LSTM Algorithm Based on Satellite Data. *IEEE Region 10 Symposium (TENSYMP)*, Mumbai, India, pp. 1-7, doi: 10.1109/TENSYMP54529.2022.9864407.

Kadir, E. A., Kung, H. T., AlMansour, A. A., Irie, H., Rosa, S. L., & Fauzi, S. S. M. (2023). Wildfire Hotspots Forecasting and Mapping for Environmental Monitoring Based on the Long Short-Term Memory Networks Deep Learning Algorithm. *Environments - MDPI*. https://doi.org/10.3390/environments10070124

Kamath, A., Vargas-Hernández, R. A., Krems, R. V., Carrington, T., & Manzhos, S. (2018). Neural networks vs Gaussian process regression for representing potential energy surfaces: A comparative study of fit quality and vibrational spectrum accuracy. *Journal of Chemical Physics*. https://doi.org/10.1063/1.5003074

La Fata, A., Moser, G., Procopio, R., Bernardi, M., & Fiori, E. (2024). A Gaussian Process Regression Method to Nowcast Cloud-to-Ground Lightning from Remote Sensing and Numerical Weather Modeling Data. *IEEE Journal of Selected Topics in Applied Earth Observations and Remote Sensing*, 1–31. https://doi.org/10.1109/JSTARS.2024.3501976

Li, J., Huang, D., Chen, C., Liu, Y., Wang, J., Shao, Y., Wang, A., & Li, X. (2024). Prediction of Forest-Fire Occurrence in Eastern China Utilizing Deep Learning and Spatial Analysis. *Forests*, *15*(9), 1672. https://doi.org/10.3390/f15091672

Li, Z., Hong, X., Kuangrong, H., Lei, C., & Biao, H. (2020). Gaussian Process Regression with heteroscedastic noises – A machine-learning predictive variance approach. *Chemical Engineering Research and Design*, *157*. https://doi.org/10.1016/j.cherd.2020.02.033

Listia Rosa, S., Abdul Kadir, E., Syukur, A., Irie, H., Wandri, R. & Fikri Evizal, M. (2022). Fire Hotspots Mapping and Forecasting in Indonesia Using Deep Learning Algorithm. *3rd International Conference on Electrical Engineering and Informatics (ICon EEI)*, Pekanbaru, Indonesia, pp. 190-194, doi: 10.1109/IConEEI55709.2022.9972281.

Luo, R., Wang, J., & Gates, I. (2024). Forecasting Methane Data Using Multivariate Long Short-Term Memory Neural Networks. *Environmental Modeling and Assessment*. https://doi.org/10.1007/s10666-024-09957-x

MacKinnon, K., & Hatta, G. (2013). *Ecology of Kalimantan: Indonesian Borneo*. Tuttle Publishing.

Madondo, R., Tandlich, R., Stoch, E., Restas, A., & Shwababa, S. (2023). Quantitative and Qualitative Data in Disaster Risk Management of Fires: A Case Study from South Africa at Various Geographical Levels. *Geographia Technica*, *18*(2), 14–39. https://doi.org/10.21163/GT_2023.182.02

Najib, M. K., Nurdiati, S., & Sopaheluwakan, A. (2021). Quantifying the joint distribution of drought indicators in Borneo fire-prone area. *IOP Conference Series: Earth and Environmental Science*. https://doi.org/10.1088/1755-1315/880/1/012002

Najib, M. K., Nurdiati, S., & Sopaheluwakan, A. (2022). Multivariate fire risk models using copula regression in Kalimantan, Indonesia. *Natural Hazards*. https://doi.org/10.1007/s11069-022-05346-3

Noh, S. H. (2021). Analysis of gradient vanishing of RNNs and performance comparison. *Information (Switzerland)*. https://doi.org/10.3390/info12110442

Nugrahani, E. H., Nurdiati, S., Bukhari, F., Najib, M. K., Sebastian, D. M., & Nur Fallahi, P. A. (2024). Sensitivity and feature importance of climate factors and evaluation of different machine learning models for predicting fire hotspots in Kalimantan, Indonesia. *IAES Int. J. Artif. Intell. (IJ-AI)*, *13*(2), 2212. https://doi.org/10.11591/ijai.v13.i2.pp2212-2225

Nurdiati, S., Bukhari, F., Julianto, M. T., Sopaheluwakan, A., Aprilia, M., Fajar, I., Septiawan, P., & Najib, M. K. (2022). The impact of El Niño southern oscillation and Indian Ocean Dipole on the burned area in Indonesia. *Terrestrial, Atmospheric and Oceanic Sciences*. https://doi.org/10.1007/S44195-022-00016-0

Nurdiati, S., Bukhari, F., Sopaheluwakan, A., Septiawan, P., & Hutapea, V. (2024). ENSO and IOD impact analysis of extreme climate condition in Papua, Indonesia. *Geographia Technica*, *19*(1), 1–18. https://doi.org/10.21163/gt_2024.191.01

Nurdiati, S., Najib, M., Bukhari, F., Revina, R., & Salsabila, F. (2022). PERFORMANCE COMPARISON OF GRADIENT-BASED CONVOLUTIONAL NEURAL NETWORK OPTIMIZERS FOR FACIAL EXPRESSION RECOGNITION. *BAREKENG: Jurnal Ilmu Matematika Dan Terapan*, *16*(3), 927–938. https://doi.org/10.30598/barekengvol16iss3pp927-938

Nurdiati, S., Sopaheluwakan, A., Julianto, M. T., Septiawan, P., & Rohimahastuti, F. (2022). Modelling and analysis impact of El Nino and IOD to land and forest fire using polynomial and generalized logistic function: cases study in South Sumatra and Kalimantan, Indonesia. *Modeling Earth Systems and Environment*. https://doi.org/10.1007/s40808-021-01303-4

Oyedele, A. A., Ajayi, A. O., Oyedele, L. O., Bello, S. A., & Jimoh, K. O. (2023). Performance evaluation of deep learning and boosted trees for cryptocurrency closing price prediction. *Expert Systems with Applications*, *213*, 119233. https://doi.org/https://doi.org/10.1016/j.eswa.2022.119233

Putra Mulia, Nofrizal, & Dewi, W. N. (2021). Analisis Dampak Kabut Asap Karhutla Terhadap Gangguan Kesehatan Fisik Dan Mental. *HEALTH CARE : JURNAL KESEHATAN*. https://doi.org/10.36763/healthcare.v10i1.103

Qirom, M. A., Rachmanadi, D., Lestari, F., & Andriani, S. (2022). Forest structure change after forest fire in peatland of Central Kalimantan. *IOP Conference Series: Earth and Environmental Science*. https://doi.org/10.1088/1755-1315/1115/1/012019

Rafhida, S. A., Nurdiati, S., Budiarti, R., & Najib, M. K. (2024). Bias correction of lake Toba rainfall data using quantile delta mapping. *CAUCHY*, *9*(2), 297–309. https://doi.org/10.18860/ca.v9i2.29124.

Rasmussen, C. E., & Williams, C. K. I. (2019). *Gaussian processes for machine learning*. MIT Press.

Reddy, C. S., Bird, N. G., Sreelakshmi, S., Manikandan, T. M., Asra, M., Krishna, P. H., Jha, C. S., Rao, P. V. N., & Diwakar, P. G. (2019). Identification and characterization of spatio-temporal hotspots of forest fires in South Asia. *Environmental Monitoring and Assessment*. https://doi.org/10.1007/s10661-019-7695-6

Saharjo, B. H., & Hasanah, U. (2023). Analisis Faktor Penyebab Terjadinya Kebakaran Hutan dan Lahan di Kabupaten Pulang Pisau, Kalimantan Tengan. *Journal of Tropical Silviculture*. https://doi.org/10.29244/j-siltrop.14.01.25-29

Saharjo, B. H., & Velicia, W. A. (2018). The Role of Rainfall Towards Forest and Land Fires Hotspot Reduction in Four Districs in Indonesia on 2015-2016. *Journal of Tropical Silviculture*. https://doi.org/10.29244/j-siltrop.9.1.24-30

Sari, R., Trihardianingsih, L., Firdaus Mulya, R., Arief, M. I., & Kusrini, K. (2022). Analisis Index Vegetation Wilayah Terdampak Kebakaran Hutan Riau Menggunakan Citra Landsat-8 dan Sentinel-2. *CogITo Smart Journal*. https://doi.org/10.31154/cogito.v8i2.439.282-294

Sarmiasih, M., & Pratama, P. Y. (2019). The Problematics Mitigation of Forest and Land Fire District Kerhutla) in Policy Perspective (A Case Study : Kalimantan and Sumatra in Period 2015-2019). *Journal of Governance and Public Policy*. https://doi.org/10.18196/jgpp.63113

Sudrajat, A. S. E., & Subekti, S. (2019). Pengelolaan Ekosistem Gambut Sebagai Upaya Mitigasi Perubahan Iklim Di Provinsi Kalimantan Selatan. *Jurnal Planologi*. https://doi.org/10.30659/jpsa.v16i2.4459

Terry, J. K., Jayakumar, M., & Alwis, K. De. (2021). Statistically Significant Stopping of Neural Network Training. *CoRR*, *abs/2103.0*. https://arxiv.org/abs/2103.01205

Ulya, N. A., & Yunardy, S. (2006). Analisis Dampak Kebakaran Hutan di Indonesia Terhadap Distribusi Pendapatan Masyarakat. *Jurnal Penelitian Sosial Dan Ekonomi Kehutanan*, *3*(2), 133–146. https://doi.org/10.20886/jpsek.2006.3.2.133-146

Van Der Werf, G. R., Randerson, J. T., Giglio, L., Van Leeuwen, T. T., Chen, Y., Rogers, B. M., Mu, M., Van Marle, M. J. E., Morton, D. C., Collatz, G. J., Yokelson, R. J., & Kasibhatla, P. S. (2017). Global fire emissions estimates during 1997-2016. In *Earth System Science Data*. https://doi.org/10.5194/essd-9-697-2017

Wasis, B., Saharjo, B. H., & Waldi, R. D. (2019). Dampak Kebakaran Hutan Terhadap Flora Dan Sifat Tanah Mineral Di Kawasan Hutan Kabupaten Pelalawan Provinsi Riau. *Journal of Tropical Silviculture*. https://doi.org/10.29244/j-siltrop.10.1.40-44

Ye, W., Alawieh, M. B., Li, M., Lin, Y., & Pan, D. Z. (2019). Litho-GPA: Gaussian Process Assurance for Lithography Hotspot Detection. *Proceedings of the 2019 Design, Automation and Test in Europe Conference and Exhibition, DATE 2019*. https://doi.org/10.23919/DATE.2019.8714960

Yuliarti, A., & Anggraini, R. N. (2022). Pengembangan Strategi Pengurangan Risiko Kebakaran Gambut Dalam Bingkai Media Berdasarkan Jumlah Hotspot Menggunakan S-Npp Viirs. *PROSIDING SEMINAR*